SUPPLEMENT NOTES

PAPER 6555, Leeman & Smith

The role of magma mixing, identification of mafic magma inputs, and structure of the underlying magmatic system at Mount St. Helens

Supplement Note 1. MSH Isotopes

Table S2 presents unpublished and published Sr, Nd, O, and Pb isotopic data and analytical information for eruptive products spanning the evolution of MSH over the last 35 ka (Leeman and others, unpublished; Halliday et al., 1983; Stern and Ito (1981). These data will be discussed in greater detail elsewhere. The point of presenting them here is that, despite small overall ranges in isotopic composition, these data illustrate (Supplement Figure S1) clear correlations amongst themselves and with SiO_2 (and other elements not shown) that support the mixing arguments made in this paper. Note that analytical errors are smaller (or, for oxygen isotopes, comparable to) data symbols in the figure. Data for the Castle Creek period span much of the compositional range, merging in composition with data for dacitic and rhyodacitic lavas erupted in previous and later cycles. Together, these data define [1] a basaltic 'end member' with mantle-like $^{87}Sr/^{86}Sr$ (~0.7030), $^{143}Nd/^{144}Nd$ (~0.5130), and $\delta^{18}O$ (~5.6‰) isotopic compositions, and [2] a silicic end member with $^{87}Sr/^{86}Sr$ (~0.704), $^{143}Nd/^{144}Nd$ (~0.51284), and $\delta^{18}O$ (~7.6‰) isotopic compositions. Smith and Leeman (1987) interpret the latter extreme as representative of partial melts of deep crustal rocks, likely of igneous origin. The former minimal extreme is representative of high-MgO (~7 wt%) basalts of both Group A and Group B as defined in this paper. In other words, despite clear differences in compositional lineages of the mafic lavas, they appear to derive from isotopically similar sources in the underlying mantle. Pb isotopic data exhibit somewhat greater scatter than the Sr and Nd data, but are distinctive for the two 'end members' with slightly more radiogenic compositions for the basalts (e.g., $^{206}Pb/^{204}Pb$ ~18.9) and less radiogenic Pb in the most silicic lavas/tephras ($^{206}Pb/^{204}Pb$ ~18.8). We also note that the oxygen isotope data are measured on whole-rock samples, and some scatter in those data could be

attributed to hydrothermal alteration; this is particularly likely for the Loowit Creek Dome for which $\delta^{18}O$ (4.6‰) is anomalously low (Halliday et al., 1983). Finally, our data for more primitive regional basalts (Leeman et al., 1990, 2004, and unpublished data) extend the arrays in Figure S1 to slightly lower $^{87}Sr/^{86}Sr$ (0.7028), $^{143}Nd/^{144}Nd$ (0.5131), and $\delta^{18}O$ (~5.3‰, on olivines), consistent with interpretations in this paper that they are representative of likely parental magmas to MSH mafic lavas.

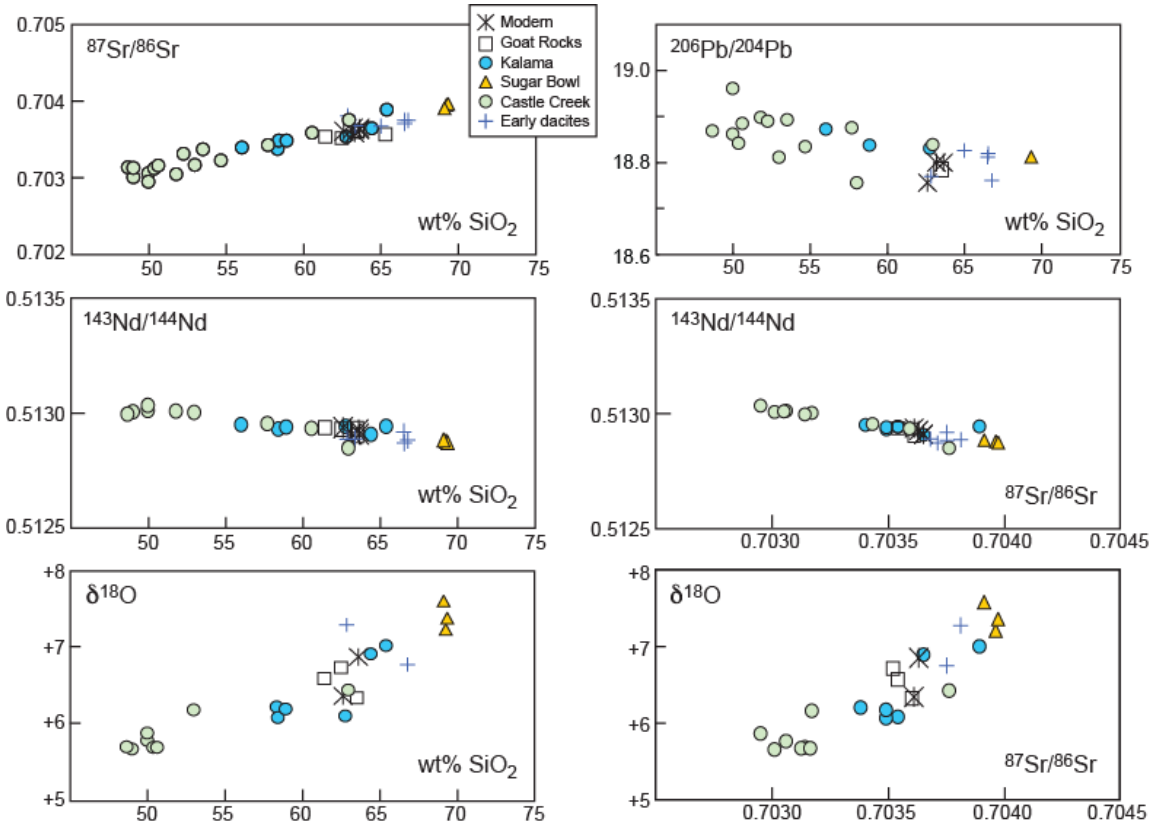

Supplement Figure S1. Variation diagrams of Sr, Pb, Nd, and O isotopes and wt% SiO_2 for MSH eruptive products. Groupings of samples are by eruptive stage in increasing age from top to bottom (cf. Pallister et al., 2017).

REFERENCES

Halliday, A.N., Fallick, A.E., Dickin, A.P., Mackenzie, A.B., Stephens, W.E., and Hildreth, W. (1983) The isotopic and chemical evolution of Mount St. Helens. Earth and Planetary Science Letters, 63, 241-256.

Smith, D.R., and Leeman, W.P. (1987) Petrogenesis of Mount St. Helens dacitic magmas. Journal of Geophysical Research, 92, 10313-10334.

Stern, R.J., and Ito, E. (1980) Incompatible element and $^{87}Sr/^{86}Sr$ compositions of Mt. St. Helens ash. Carnegie Institute of Washington Yearbook, 79, p. 486.

Supplement Note 2. Magmatic end-members

Bulk compositions

Table S3 presents average compositions for relevant local magma types, including MSH andesitic and dacitic eruptive products, and regional mafic lavas with at least 7.5 wt% MgO. The latter include LKT, ne-IPB and hy-IPB (both similar to ocean island basalts), normal (CAB) and high-K (HKCA) calcalkalic basalts (cf. Smith and Leeman, 1987, 1993; Leeman et al., 1990, 2005, and unpublished). The average MSH andesite and LKT, ne-IPB, and hy-IPB compositions are used in mixing calculations described in Table S5. Also included in Supplement Table S3 are averages of MSH basalt sub-types: Groups A, B1 and B2. These are considered to derive from distinct domains in the magmatic plexus underlying MSH, and are used in constructing Supplement Figures A3 and A4 (also cf. Table S5).

Olivine core compositions

For comparison with MSH olivine populations, we show here (Supplement Figure S2) the ranges in olivine core compositions measured in representative regional primitive basaltic lavas (analytical data given in Tables 1 and 2). Samples are from the Indian Heaven lava field (LKT, DS-80A-80; hy-IPB, DS-6A-80; ne-IPB, DS49A-80; and SHO, DS-42-81), and from the far frontal arc Battleground lava field (ne-IPB, PB-9). Despite the relatively high Mg#s for these lavas, the range in core compositions is about 8 mol% Fo for the primitive LKT, and approximately 10-15 mol% Fo for the others. Thus, we infer that even these relatively primitive lavas have potentially experienced some modification during ascent and storage at deep crustal depths.

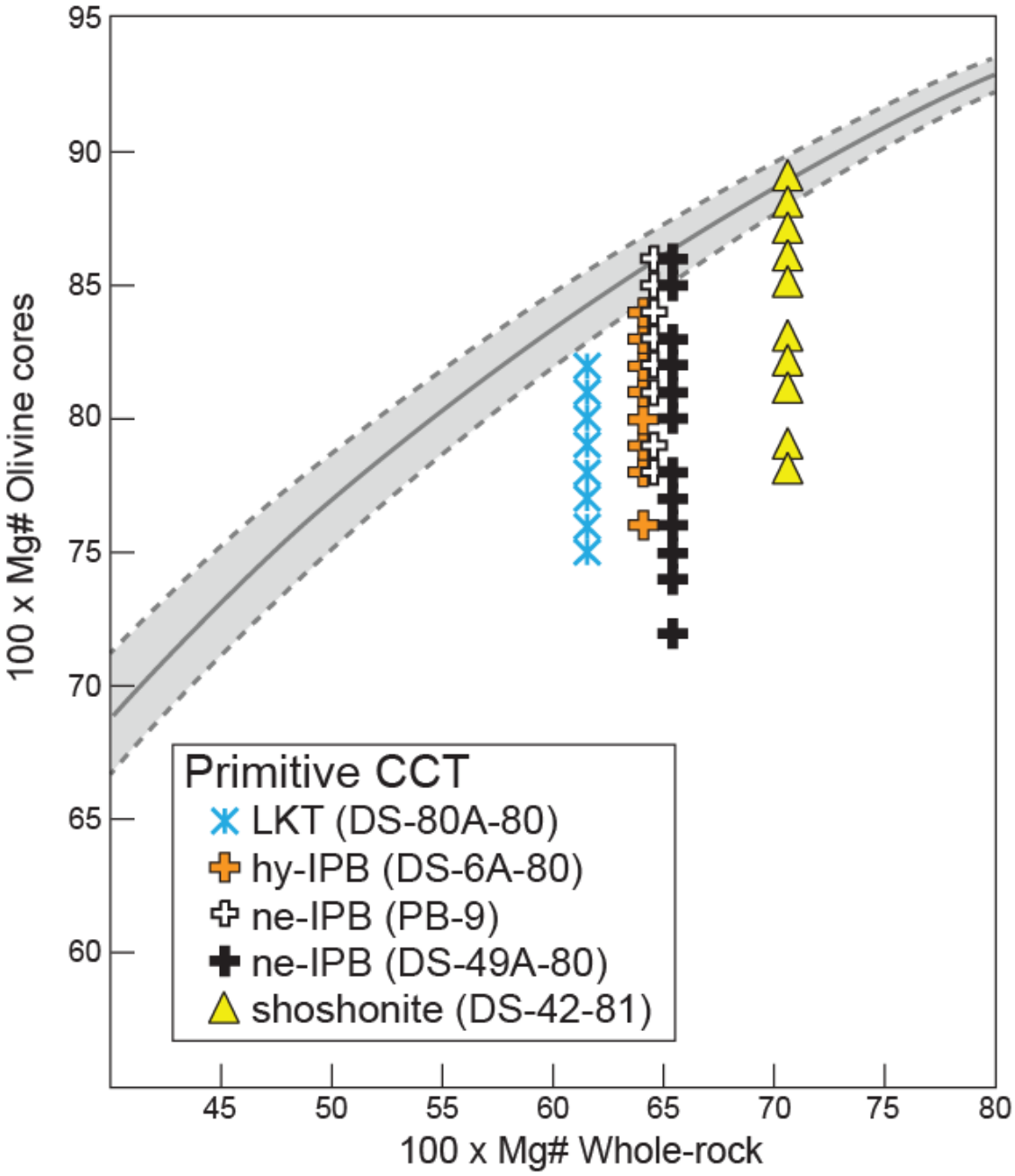

Supplement Figure S2. Rhodes diagrams for selected primitive basalts from the CCT, which are considered potentially parental to more evolved MSH counterparts.

REFERENCES

Leeman, W.P., Smith, D.R., Hildreth, W., Palacz, Z., and Rogers, N. (1990) Compositional diversity of Late Cenozoic basalts in a transect across the southern

Washington Cascades: Implications for subduction zone magmatism. Journal of Geophysical Research, 95, 19561-19582.

Leeman, W.P., Lewis, J.F., Evarts, R.C., Conrey, R.M., and Streck, M.J. (2005) Petrologic constraints on the thermal structure of the Cascades arc. Journal of Volcanology and Geothermal Research, 140, 67-105.

Smith, D.R., and Leeman, W.P. (1987) Petrogenesis of Mount St. Helens dacitic magmas. Journal of Geophysical Research, 92, 10313-10334.

Smith, D.R., and Leeman, W.P. (1993) The origin of Mount St. Helens andesites. Journal of Volcanology and Geothermal Research, 55, 27-303, doi:10.1016/0377-0273(93)90042-P.

Supplement Note 3. Fractional crystallization models

Supplement Table S4 presents simple fractional crystallization (FC) models that show expected compositional trends (see text Fig. 13) assuming removal of observed phenocrysts (olivine and plagioclase) from the highest-MgO basalts of Groups A and B1. Two models are shown corresponding to olivine:plagioclase ratios of 0.3:0.7 (late stage, similar to phenocryst proportions in Group A, Cave basalt) and 0.9:0.1 (early stage, olivine dominant) for crystal removal. For the major and trace elements shown, partition coefficients were adopted from Leeman and Scheidegger (1977) and Laubier et al. (2014) for olivine, and Tepley et al. (2010) and Laubier et al. (2014) for plagioclase.

As discussed in the text, all incompatible elements (see representative plots for La, Nb, Th, Ba, Sc and Sr; right side of Supplement Table S4 spreadsheet, cell T15) display patterns in MSH mafic lavas similar to those in text Figure 13. Comparison with the calculated FC curves demonstrates that this process cannot explain the observed trends, albeit FC could contribute to some dispersion of the data. Similarly, the compatible element Ni decreases with MgO to a lesser degree than predicted by the FC curves, and in fact defines a quasi-linear array consistent with mixing between basalt and more evolved magmatic components. The variation of compatible Cr is ambiguous, but if we subtract small amounts of Cr-spinel (which occurs as inclusions in many MSH olivines), FC curves for this element will likely resemble those for Ni (i.e., decrease with MgO more rapidly than observed).

Note that although the plots of MgO vs. CaO, Cr, and Sc are arguably consistent with magma mixing, they are also permissive of removal of minor amounts of clinopyroxene. This mineral was not included in the FC models because it only occurs as a trace phenocryst in a few MSH (Group B) basaltic lavas; its incorporation at low modal proportions would not significantly alter the model outcomes.

REFERENCES

Laubier M., Grove T.L., and Langmuir C. H. (2014) Trace element mineral/melt partitioning for basaltic and basaltic andesitic melts: an experimental and laser ICP-

MS study with application to the oxidation state of mantle source regions. Earth and Planetary Science Letters, 392, 265–278, doi:10.1016/j.epsl.2014.01.053.

Leeman, W.P., and Scheidegger, K.F. (1977) Olivine/liquid distribution coefficients and a test for crystal-liquid equilibrium. Earth and Planetary Science Letters, 35, 247-257, doi:10.1016/0012-821X(77)90128-5.

Tepley, F.J., III, Lundstrom, C.C., McDonough, W.F., and Thompson, A. (2010) Trace element partitioning between high-An plagioclase and basaltic to basaltic andesite melt at 1 atmosphere pressure. Lithos, 118, 82-94, doi:10.1016/j.lithos.2010.04.001.

Supplement Note 4. Mixing models

Previous work on MSH eruptive products has demonstrated the importance of magma mixing processes at this volcano. Pallister et al. (1992) demonstrate a range of mixing arrays for andesites and dacites of the Kalama (1479-1750 C.E.), Goat Rocks (1800-1857 C.E.), and modern eruptive episodes (1980-present); basaltic magmas have not so far been documented in these younger eruptive episodes. Smith and Leeman (1993) presented chemical and mineralogical evidence that many MSH andesites themselves could have been produced by mixing between ascending basalt and more evolved dacitic to rhyodacitic magmas, with the latter interpreted to be melts of crustal lithologies of igneous origin (Smith and Leeman, 1987). It appears that, over time and/or space, compositions of potential mixing components in the feeder system varied, and may themselves comprise products of complex mixing between intermittent fresh inputs from the mantle (basalts), partial melts of preexisting crust (including earlier Cascades magmatic rocks), prior mixing hybrids, and differentiated (more evolved) liquids derived from any of the above (cf. Pallister et al., 2008; Cooper and Donnelly, 2008; Carroll et al., 2008, 2009; Lieuallen, et al., 2009; Claiborne et al., 2010). On the other hand, the coherent Castle Creek mixing arrays discussed in this paper suggest that stored magmatic components in the feeder system apparently were relatively homogeneous over the brief duration of this episode, at least at depths intersected by the ascending basaltic magmas.

Supplement Table S5 presents calculated mixing proportions for the three hypothetical basalt-andesite mixing arrays shown in text Figure 13. Mafic end members are primitive LKT basalt average (assumed Group A parent; trend M1), ne-IPB average (assumed Group B1 parent; trend M2), and hy-basalt average (assumed Group B2 parent; trend M3). These are all assumed to mix with material similar to MSH average andesite. Compositions of each end member can be found in Supplement Table S3. We note that in text Figure 13 an andesitic end member with MgO near 5 wt% and K_2O near 1 wt% would more closely produce linear arrays for trends M1, M2, and M3. However, the average andesite was used as it serves as a more plausible mixing end-member when considering all elements.

Major element mixing results are shown in Supplement Table S5 for representative lavas from the respective groups that approximate the three trends in text Figure 13. Included are the calculated weight fraction (X-a) of the andesitic additive, sum of the 'residuals squared' for all major elements, and comparison of observed and back-calculated MgO contents for each sample. Plots show the relations between X-a and the actual observed MgO in each sample. Values of ∑(R^2) highlighted in yellow reflect poor fits, and these samples are omitted from the plots. Overall, the mixing models are reasonable approximations, but scatter in trend M3 in particular indicates that many of these samples likely have a more complex evolution than simple mixing of the two end members considered here. Possible causes for this scatter are variance in the assumed end member compositions, and perhaps inclusion of samples into mixing groups that are not all related to the same evolutionary pathways. Bold and italicized sample names indicate those used in trace element evaluations of the mixing models (cf. Supplement Figure S3).

The major element mixing models have been evaluated using trace element and Sr isotopic data. Trace element compositions of hypothetical mixtures were calculated using the aforementioned mixing proportions estimated for individual samples. For this test we rely on samples for which trace element contents are most comprehensive. Calculated compositions are normalized to observed compositions, and averages of these ratios reported for the selected samples. Considering uncertainties in [a] analytical data, [b] choice of mixing end members, and [c] mixing proportions, ratios within ± 20% of unity (i.e., values between 0.8 and 1.2) are deemed supportive of the estimated mixing proportions. Averages of these values for individual samples are within this range for most samples. Results are shown graphically in Supplement Figure S3.

Finally, we also used the estimated mixing proportions to calculate Sr isotope mixing trajectories for mixing trends M1, M2, and M3 (see plots in Supplement Table S5). These calculations include weightings for Sr contents in the mixing end members. Acceptable mixing arrays that fit available isotopic data are obtained as long as the basaltic input magmas have $^{87}Sr/^{86}Sr$ ratios near 0.70295-0.70300. In particular, the hy-IPB average $^{87}Sr/^{86}Sr$ value is significantly higher than this value, but it is based on few analyses and therefore may not be representative. We also note that mixing trajectories

hinge on the ratio of Sr contents between mixing end members. The M1 mixing array is significantly improved by using a 25% lower Sr content than the actual average for the LKT end member. Other isotopic data will be evaluated in another, more detailed paper.

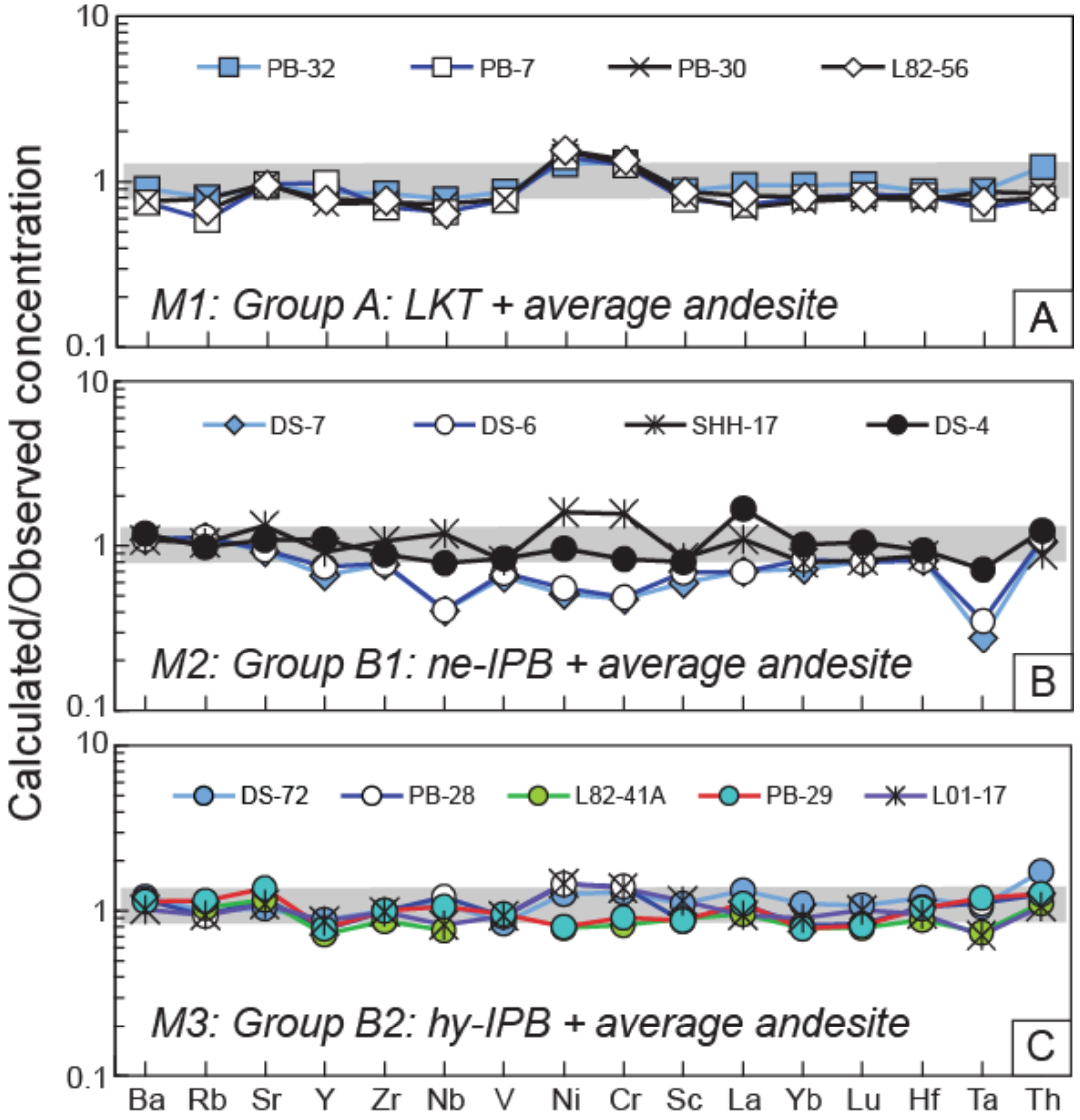

Supplement Figure S3. Trace element evaluation of major element-based mixing models. Abundances of trace elements are calculated for each sample based on estimated mixing proportions (Supplement Table S5) and compositions (Supplement Table S3) of the mixture end members; these are normalized to the actual sample composition. M1, M2, M3 correspond to the hypothetical trends shown in text Figure 13. Gray fields indicate probable errors (ca. ± 20%) considering uncertainties in analytical data, in choice of mixing end members, and in mixing proportions.

REFERENCES

Carroll, K.R., Streck, M.J., Pallister, J.S., and Leeman, W.P. (2008) Interaction of dacitic and basaltic magmas deduced from evolution of phenocrysts and mixing of crystal populations during the Kalama eruptive period, Mount St. Helens. American Geophysical Union, Fall Meeting 2008, Abstract id. V23E-2175.

Carroll, K.R., Streck, M.J., Pallister, J.S., and Leeman, W.P. (2009) Mixing components and hybridization processes of Kalama period intermediate magmas from Mount St. Helens: Evidence from mafic phenocrysts. Geological Society of America Abstracts with Programs, 41, no. 7, 190.

Claiborne, L.L., Miller, C.F., Flanagan, D.M., Clynne, M.A., and Wooden, J.L. (2010) Zircon reveals protracted magma storage and recycling beneath Mount St. Helens. Geology, 38, 1011-1014.

Cooper, K.M., and Donnelly, C.T. (2008) ^{238}U-^{230}Th-^{226}Ra disequilibria in dacite and plagioclase from the 2004-2005 eruption of Mount St. Helens. In D.R. Sherrod, W.E. Scott, W.E., and P.H. Stauffer, Eds., A volcano rekindled: The renewed eruption of Mount St. Helens, 2004–2006. U.S. Geological Survey Professional Paper 1750, p. 827-846.

Lieuallen, A.E., Tepley, F.J., and Clynne, M.A. (2009) Magmatic interactions on short time scales: magma mixing during the Kalama eruptive period at Mount St. Helens, Washington. American Geophysical Union, Fall Meeting 2009, Abstract id. V43B-2239.

Pallister, J.S., Hoblitt, R.P., Crandell, D.R., and Mullineaux, D.R. (1992) Mount St. Helens a decade after the 1980 eruptions: Magmatic models, chemical cycles, and a revised hazards assessment. Bulletin of Volcanology, 54, 126-146.

Pallister, J.S., Thornber, C.R., Cashman, K.V., Clynne, M.A., Lowers, H.A., Mandeville, C.W., Brownfield, I.K., and Meeker, G. (2008) Petrology of the 2004-2006 Mount St. Helens lava dome: Implications for magmatic plumbing and eruption triggering. In D.R. Sherrod, W.E. Scott, W.E., and P.H. Stauffer, Eds., A volcano rekindled: The renewed eruption of Mount St. Helens, 2004–2006. U.S. Geological Survey Professional Paper 1750, p. 647-702.

Smith, D.R., and Leeman, W.P. (1987) Petrogenesis of Mount St. Helens dacitic magmas. Journal of Geophysical Research, 92, 10313-10334.

Smith, D.R., and Leeman, W.P. (1993) The origin of Mount St. Helens andesites. Journal of Volcanology and Geothermal Research, 55, 27-303, doi:10.1016/0377-0273(93)90042-P.

Supplement Note 5. P-T-H_2O calculations

Pressure and temperature conditions for MSH magmas were estimated based on unmodified compositions of individual lava samples using silica-activity barometry and olivine-liquid thermometry as described by Putirka (2008, 2016) and Lee et al. (2009). This approach essentially depends on the assumption that whole-rock compositions approximate those of magmatic liquids, and this is supported by the generally low (<15%) phenocryst content of most MSH basaltic lavas. We also note that alternative approaches to barometry based on clinopyroxene-liquid equilibria (cf. Neave and Putirka, 2017) are generally not applicable to MSH basalts owing to the absence of true pyroxene phenocrysts in most samples. For the same reason, pressure estimates based on loci of the ol + pl + cpx + melt (OPAM) cotectic (cf. Kelley and Barton, 2008) are of uncertain validity, but are shown for comparison with other methods; we note that this phase equilibria approach is also affected by magmatic water content and this introduces additional uncertainty in pressure estimates (cf. Michael and Cornwall, 1998; Husen et al., 2016).

For convenience of comparison, results are shown for individual samples in Supplement Table S6; these include both olivine-liquid and plagioclase-liquid models. Temperatures and pressures are reported based on all of the thermobarometry algorithms discussed by the aforementioned papers as well as the thermometer of Sugawara (2000). Critical parameters for these calculations include redox state and water contents of the respective magmas. Based on olivine-spinel equilibria for representative samples, Smith and Leeman (2005) estimated that X-fe3 (=$Fe^{3+}/[Fe^{3+} + Fe^{2+}]$, cation basis) is approximately 0.15 for MSH mafic lavas; this corresponds to oxygen fugacity slightly more oxidized than the QFM redox buffer. This inference is also supported by V/Sc and Zn/Fe systematics in primitive basalts from MSH and environs (Lee et al., 2005; 2010; also see Tang et al., 2018). Lacking detailed mineral chemistry for all samples, this value of 0.15 is used in all calculations here. Water contents have been measured directly in olivine-hosted melt inclusions from only a few MSH mafic tephras (cf. main text; Rea et al., 2012). These data are augmented here using the plagioclase-liquid hygrometers of Waters and Lange (2015) and Putirka (2005). Accuracy of these hygrometers is

nominally ± 0.35 wt% and ± 1.0 wt%, respectively, and relative differences for MSH lavas are comparable (cf. Table S6, cell T140). It should be noted that several of the thermometers are pressure sensitive, and vice versa for some barometers, and some of these are also sensitive to magmatic water content. In practice, where pressure input is required, we initially plugged in the Lee et al. (2009) pressure estimate because this parameter is computed independent of a temperature variable. Resulting temperature estimates and the Lee et al. pressure were input into the Waters and Lange hygrometer to arrive at preliminary estimates of water content. These were then included in the respective lava compositions, and the process was repeated; after three iterations, values for T, P, and H_2O content stabilized, and these latter results are reported for each algorithm in Supplement Table S6. Finally, magma densities are presented for each sample on both hydrous and anhydrous bases as calculated according to Bottinga and Weill (1970). In these calculations, we use volume and thermal expansion data from Lange and Carmichael (1987), compressibility data from Kress and Carmichael (1991), and water contents estimated in this paper.

Regarding the hygrometers, the veracity of water estimates technically hinges on knowledge of equilibrium compositions of melt and plagioclase, both of which have inherent uncertainties that are difficult to define precisely. In all cases, we assume that liquid compositions are represented by the whole-rock analyses. Preliminary work on olivine-hosted melt inclusions from primitive CCT basalts indicates that this is often the case (Rowe et al., 2009, Leeman et al., unpublished data). However, to the extent that the bulk rocks are actually mixtures, it is possible that the real liquids are somewhat more evolved than the whole rock composition. Feldspar compositions can be inferred from analyses of prevalent plagioclase phenocryst populations in the few samples studied in detail. Based on available data, the plagioclases are rarely more calcic than An_{82}, but do range to more sodic compositions as low as An_{60} in some samples, generally decreasing with bulk rock SiO_2 content. We initially evaluated the effects of varied An content on calculated intensive parameters and water contents by using a range of feldspar compositions appropriate for individual samples.

Effects on water estimates were evaluated for all input parameters (see detailed results for sample PB-32 in Table S6; cell C120). For example, holding P and T constant, a

range of 22 mol% An content (An_{82-60}) corresponds to a range in estimated water content from 1.0 to 0.6 wt% (2.6% relative per mol% An). Similarly, holding other variables constant, a 0.4 GPa range in pressure (0.5-0.9 GPa) corresponds to a range in H_2O of less than 10% relative (0.67-0.74 wt%), whereas a 20°C range in temperature (1181°-1201°C) changes water content by 36% relative (0.58-0.84 wt%). Although temperature has the largest effect on water estimates, the availability of reliable temperature estimates (as discussed below) minimizes this source of uncertainty. Finally, considering the relatively small effect of pressure on water estimates, the most critical remaining unknown is An content of equilibrium plagioclase.

We evaluated this parameter in the following way. Given the strong dependence of the Putirka (2008; equation [25a]) plagioclase barometer on feldspar composition, we estimated an 'optimal' plagioclase composition by graphically determining the X_{An} value for which both the Lee et al. (2009) and Putirka (2008) barometers yield equivalent pressures for individual samples (cf. plots of P vs. X_{An} in Table S6, cell BK108). The resulting 'optimal' plagioclase compositions are in the range An_{70}-An_{60} for MSH basaltic lavas. These estimates generally lie within the range observed in the dominant phenocryst populations, but are skewed toward the sodic end of the range for any given sample. However, they may better approximate the actual equilibria involved in mixed or hybrid magmas. The question of equilibrium phase compositions is a widespread issue that remains unresolved. Our approach at least produces close convergence between multiple thermometers and barometers on a common set of samples.

For thermometry, estimates based on olivine-liquid equilibrium are considered more robust than the so-called 'liquid' thermometers. Of these, results for each sample using the models of Lee et al. (2009) and Sugawara (2000), and those discussed by Putirka (2008), agree closely. The sample by sample averages of seven of the eight such thermometers evaluated have a mean S.D. of only 11°C. Only results using the thermometer of Putirka (2008; equation [9]) are excluded from the average for each sample because they are systematically higher (by 58°C on average). Overall, this agreement is far better than the nominal uncertainties (± 20°C at best) expected for these thermometers. And notably, the plagioclase-saturation thermometer of Putirka (2008, equation [26]) agrees closely with the 'liquid' and 'olivine-liquid' thermometers, as do

the 'plagioclase-liquid' thermometers (Putirka, 2008, equations [23] and [24a]); however, because the latter are in most cases based on estimated plagioclase compositions, they are omitted from the overall averages for each sample. Despite this, we note that average plagioclase-based Ts differ from average olivine/liquid-based temperatures by no more than 16°C (with mean Δ = 10°C). For convenience in subsequent discussion, we adopted the Lee et al. (2009) temperature estimates as representative; these are on average 1°C higher than average olivine/liquid-based Ts and 9°C lower than average plagioclase-based Ts.

For barometry, we show results for algorithms of Kelley and Barton (2008), Lee et al. (2009), and also Putirka (2008, 2016) for both silica activity and plagioclase-liquid models. Pressure estimates using the approach of Kelley and Barton (2008) are generally lower and overlap to some extent for Group A and B1 basalts (SiO_2 <53%). The silica activity models of Lee et al. (2009) and Putirka (2016) are both considered to be well calibrated by laboratory experiments. In applying these barometers to the natural MSH samples, the greatest concern is the paucity of extant pyroxene phenocrysts. However, trends of decreasing Cr and Sc with decreasing MgO (cf. plots in Supplement Table S4) may signify cryptic removal of pyroxenes as the magmas evolved.

To evaluate the accuracy of these barometers, we selected 90 experiments (see list of sources below) from the Library of Experimental Phase Relations (LEPR) database (Hirschmann et al., 2008) for which melts were multiply-saturated (liq + oliv ± opx ± cpx ± plag) and redox conditions were reasonably well-known. As discussed in detail by Putirka (2016), experiments lacking pyroxene do not adequately buffer silica activity upon which the barometers are theoretically based, and were therefore excluded from consideration. Considering the range of pressures estimated for MSH lavas, we also restricted our selection of experimental data to $0.1 \leq P \leq 1.5$ GPa (0.1 - 1.5 GPa). Oxygen fugacities were calculated for each run, and melt compositions were recalculated using the corresponding X-fe3 values (based on equation [7] of Putirka, 2016) to obtain realistic FeO and Fe_2O_3 contents. These X-fe3 estimates closely match those calculated using the methods of Kress and Carmichael (1991) and Berry et al. (2018, and personal communication). Comparison of calculated vs. experimental pressures is shown in Supplement Table S6. In this diagram, calculated pressures based on the two barometers

can be compared for the same experiments. Averages and standard deviations for the two are shown below for multiple experiments carried out at four representative pressures. These comparisons indicate that the Putirka barometer tends to produce systematically higher estimates for the pressure range of interest.

Because pressure estimates based on the Lee et al. (2009) barometer more closely match the nominal experimental pressures and exhibit somewhat less variance, they are adopted for discussion in this paper. Also, as discussed in the text, they accord well with other geologic constraints. However, considering the dispersion of calculated pressures, estimates based on only a few samples may have a large uncertainty (in some cases exceeding 0.5 GPa); this may be considerably reduced where a large number of samples produce consistent estimates (cf. Putirka, 2008), as is the case for MSH lavas.

Supplement Table S6 presents a summary of average T, P, and equivalent depth for the distinct compositional groups of MSH lavas. For internal consistency, these averages are based on estimates using the Lee et al. (2009) thermobarometer. It is important to note that relative differences in physical conditions for these groups would be similar, albeit slightly higher in pressure, using the Putirka (2016) barometer. As discussed in the text, the inferred physical conditions are highly correlated with compositional variations (cf. plots in Supplement Table S6, and text Figure 14).

Average pressures calculated for selected isobaric experiments (P-exp)

P-exp (GPa)	0.50	0.75	0.88	1.00
P-Put	0.51 ± 0.36	1.09 ± 0.05	1.08 ± 0.09	1.11 ± 0.20
P-Lee	0.47 ± 0.07	0.90 ± 0.08	0.75 ± 0.09	1.01 ± 0.15
N	5	7	15	48

Sources of experimental data used in this comparison*:* N = number of experiments evaluated

[1] Baker, R.B., and Eggler, D.H. (1987) Compositions of anhydrous and hydrous melts coexisting with plagioclase, augite, and olivine or low-Ca pyroxene from 1 atm to 8 kbar: Applications to the Aleutian volcanic center of Atka. American Mineralogist, 72, 12-28. [n=7]

[2] Baker, M.B., and Stolper, E.M. (1994) Determining the composition of high-pressure mantle melts using diamond aggregates. Geochimica et Cosmochimica Acta, 58, 2811-2827. [n=5]

[3] Bulatov, V.K., Girnis, A.V., and Brey, G.P. (2002) Experimental melting of a modally heterogeneous mantle. Mineralogy and Petrology, 75, 131-152. [n=12]

[4] Grove, T.L., Kinzler, R.J., and Bryan, W.B. (1992) Fractionation of mid-ocean ridge basalts. In J.P. Morgan, D.K. Blackman, and J.M. Sinton, J.M., Eds., Mantle flow and melt generation at mid-ocean ridges. Geophysics Monograph 71, American Geophysical Union, Washington, D.C., p. 281-310. [n=12; experiments at T ≥ 1200°C]

[5] Kawamoto, T. (1996) Experimental constraints on differentiation and H_2O abundance of calc-alkaline magmas. Earth and Planetary Science Letters, 144, 577-589. [n=3]

[6] Kägi, R., Müntener, O., Ulmer, P., and Ottolini, L. (2005) Piston-cylinder experiments on H_2O undersaturated Fe-bearing systems: An experimental setup approaching fO_2 conditions of natural calc-alkaline magmas. American Mineralogist, 90, 708-717. [n=7]

[7] Medard, E., and Grove, T.L. (2007) The effect of H_2O on the olivine liquidus of basaltic melts: Experiments and thermodynamic models. Contributions to Mineralogy and Petrology, 155, 417-432. [n=1]

[8] Pichavant, M., Mysen, B.O., and MacDonald, R. (2002) Source and H_2O content of high-MgO magmas in island arc settings: An experimental study of a primitive calc-alkaline basalt from St. Vincent, Lesser Antilles arc. Geochimica et Cosmochimica Acta, 66, 2193-2209. [n=4]

[9] Pickering-Witter, J., and Johnston, A.D. (2000) The effects of variable mineral proportions on the melting systematics of fertile peridotite assemblages. Contributions to Mineralogy and Petrology, 140, 190-211. [n=10]

[10] Putirka, K., Johnson, M., Kinzler, R., Longhi, J., and Walker, D. (1996) Thermobarometry of mafic igneous rocks based on clinopyroxene-liquid equilibria. Contributions to Mineralogy and Petrology, 123, 92-108. [n=4]

[11] Schwab, B.E., and Johnston, A.D. (2001) Melting systematics of modally variable, compositionally intermediate peridotites and the effects of mineral fertility. Journal of Petrology, 42, 1789-1811. [n=7]

[12] Scoates, J.S., Lo Cascio, M., Weis, D., and Lindsley, D.H. (2006) Experimental constraints on the origin and evolution of mildly alkalic basalts from the Kerguelen Archipelago, southeast Indian Ocean. Contributions to Mineralogy and Petrology, 151, 582-599. [n=1]

[13] Stolper, E. (1980) A phase diagram for mid-ocean ridge basalts: Preliminary results and implications for petrogenesis. Contributions to Mineralogy and Petrology, 74, 13-27. [n=1]

[14] Villiger, S., Ulmer, P., Müntener, O., and Thompson, A.B. (2004) The liquid line of descent of anhydrous, mantle-derived, tholeiitic liquids by fractional and equilibrium crystallization – an experimental study at 1.0 GPa. Journal of Petrology, 45, 2369-2388. [n=1]

[15] Wasylenki, L.E., Baker, M.B., Kent, A.J.R., and Stolper, E.M. (2003) Near-solidus melting of the shallow upper mantle: Partial melting experiments on depleted peridotite. Journal of Petrology, 44, 1163-1191. [n=8]

[16] Whitaker, M.L., Nekvasil, H., Lindsley, D.H., and Difrancesco, N.J. (2007) The role of pressure in producing compositional diversity in intraplate basaltic magmas, Journal of Petrology, 43, 365-393. [n=7]

Summary and concluding caveats

[1] Strictly, the Lee et al. algorithm applies only to melts saturated with olivine and one or more pyroxenes. Thus, pressure or temperature estimates for any lava less mafic than basaltic andesite should be treated with caution. This may be the case for some of the other olivine-based thermobarometers compiled in the worksheet. However, these do seem to give reasonable agreement as long as there is actually olivine in the liquid.

[2] Despite the previous caveat, it is remarkable how well all of the olivine-based thermometers agree. As we noted, the Lee et al results are within a few degrees of the average for all but one of Putirka's thermometers, and this justifies our reliance on the Lee et al values. Essentially, all but one are interchangeable. And regarding more

evolved lavas, we note the close agreement between the thermometers used across the entire magma compositional spectrum that we considered.

[3] Calculated pressures were tested against a large number of experiments for which the appropriate phase assemblages exist, as described above. We also compare P estimates for our MSH mafic lavas using three different barometers in histograms near cell C141. Lee et al. values are generally intermediate between estimates by Putirka (2016) [slightly higher] and Kelley & Barton (2008) [slightly lower], and the Lee et al. estimates seem more uniform within distinct subsets of the mafic lavas.

[4] We explicitly evaluated effects of uncertainties in P, T, or X-An on water estimates for the Waters & Lange hygrometer, as shown in a Table near cell C120. These are compared with results of the Putirka (2005) hygrometer, which has larger nominal uncertainties, near cell T139. Interestingly, the two methods actually converged during the iterative substitution of water estimates.
We note that that our water estimates seem low for andesitic or more evolved magmas. This could reflect overestimation of T where based on the thermometers we used. On the other hand, lower temperatures based for example on Fe-Ti oxide thermometry could underestimate magmatic Ts, especially if the oxides crystallize late, as in groundmass.

[5] Explicit ranges in water content are presented for each sample assuming maximum, intermediate, and minimum An in plag (based on actual analyses of representative samples) and also the 'optimum' X-An (discussed above). See lines 92-103. Also, note the close agreement between plagioclase thermometry and olivine-based thermometry; cf. lines 42, 45 and 48-50.

[6] Lastly, we note that the issue of what is the actual equilibrium plagioclase composition is not a trivial one. The actual mineral populations likely include a range of compositions reflecting temperature variations and potential mixing with different magmas during ascent and storage (i.e., not unlike the variations we documented in the

olivine populations). This is the reason we tried to estimate 'optimal' compositions for the feldspars. To some extent, this issue also may be relevant for other mineral species.

REFERENCES

Berry, A.J., Stewart, G.A., O'Neill, H.S.C., Mallmann, G., and Mosselmans, J.F.W. (2018) A re-assessment of the oxidation state of iron in MORB glasses. Earth and Planetary Science Letters, 483, 114-123, doi:10.1016/j.epsl.2017.11.032.

Bottinga, Y., and Weill, D. F. (1970) Densities of liquid silicate systems calculated from partial molar volumes of oxide components. American Journal of Science, 269, 169-182.

Hirschmann, M.M., Ghiorso, M.S., Davis, F.A., Gordon, S.M., Mukherjee, S., Grove, T.L., Krawczynski, M., Medard, E., and Till, C.B. (2008) Library of Experimental Phase Relations (LEPR): A database and Web portal for experimental magmatic phase equilibria data. Geochemistry, Geophysics, and Geosystems, 9, Q03011, doi:10.1029/2007GC001894.

Husen, A., Almeev, R.R., and Holtz, F. (2016) The effect of H_2O and pressure on multiple saturation and liquid lines of descent in basalt from the Shatsky Rise. Journal of Petrology, 57, 309-344, doi:20.2093/petrology/egwoo8.

Kelley, D.F., and Barton, M. (2008) Pressures of crystallization of Icelandic magmas. Journal of Petrology, 49, 465-492, doi:10.1098/petrology/egm089.

Kress, V.C. and Carmichael, I.S.E. (1991) The compressibility of silicate liquids containing Fe_2O_3 and the effect of composition, temperature, oxygen fugacity and pressure on their redox states. Contributions to Mineralogy and Petrology, 108, 82–92.

Lange R.A. and Carmichael I.S.E. (1987) Densities of Na_2O–K_2O–CaO–MgO–FeO–Fe_2O_3–$A1_2O_3$–TiO_2–SiO_2 liquids: new measurements and derived partial molar properties. Geochimica et Cosmochimica Acta, 51, 2931–2946.

Lee, C.-T.A., Leeman, W.P., Canil, D., and Li, Z.A. (2005) Similar V/Sc systematics in MORB and arc basalts: Implications for the oxygen fugacities of their mantle source regions. Journal of Petrology, 46, 2313-2336, doi:10.1093/petrology/egi056.

Lee, C.-T.A., Luffi, P., Plank, T., Dalton, H., and Leeman, W.P. (2009) Constraints on the depths and temperatures of basaltic magma generation on Earth and other terrestrial planets using new thermobarometers for mafic magmas. Earth and Planetary Science Letters, 279, 20-33.

Lee, C.-T.A., Luffi, P., Le Roux, V., Dasgupta, R., Albaréde, F., and Leeman, W.P. (2010) The redox state of arc mantle using Zn/Fe systematics. Nature, 468, 681-685, doi: 10.1038/nature09617.

Michael, P.J., and Cornell, W.C. (1998) Influence of spreading rate and magma supply on crystallization and assimilation beneath mid-ocean ridges: Evidence from chlorine and major element chemistry of midocean ridge basalts. Journal of Geophysical Research, 103, 18325–18356.

Neave, D.A., and Putirka, K.D. (2017) A new clinopyroxene-liquid barometer, and implications for magma storage pressures under Icelandic rift zones. American Mineralogist, 102, 777-794, doi:10.2138/am-2017-5968.

Putirka, K.D. (2008) Thermometers and barometers for volcanic systems. Reviews in Mineralogy and Geochemistry, 69, 61-120.

Putirka, K. (2016) Rates and styles of planetary cooling on Earth, Moon, Mars, and Vesta, using new models for oxygen fugacity, ferric-ferrous ratios, olivine-liquid Fe-Mg exchange, and mantle potential temperature. American Mineralogist, 101, 819-840, doi:10.2138/am-2016-5402.

Rea, J., Wallace, P.J., and Clynne, M.A. (2012) Pre-eruptive volatile content of mafic magma from the 2.0-1.7 ka Castle Creek eruptive period, Mount St. Helens**.** EOS, American Geophysical Union, Abstract V53C-2853.

Smith, D.R., and Leeman, W.P. (2005) Chromian spinel-olivine phase chemistry and the origin of primitive basalts of the southern Washington Cascades. Journal of Volcanology and Geothermal Research, 140, 49-66.

Sugawara, T. (2000) Empirical relationships between temperature, pressure, and MgO content in olivine and pyroxene saturated liquid. Journal of Geophysical Research, 105, 8457-8472.

Tang, M., Erdman, M., Eldridge, G., and Lee, C.-T.A. (2018) The redox "filter" beneath magmatic orogens and the formation of continental crust. Science Advances, 4, eaar4444, doi: 10.1126/sciadv.aar4444.

Waters, L.E., and Lange, R.A. (2015) An updated calibration of the plagioclase-liquid hygrometer-thermometer applicable to basalts through rhyolites. American Mineralogist, 100, 2172-2184.

Supplement Note 6. Trace element comparisons of MSH and primitive CCT basalt types

To further assess genetic relationships between input magmas, we consider the relative compositions of selected end members (Supplement Figure S4; averages used are given in Supplement Table S3). Comparing ne-IPB and hy-IPB end members to the LKT average, it is clear that all incompatible elements (e.g., Rb to Hf in Supplement Fig. S4) are systematically enriched in IPB lavas. Because there is no obvious preferential enrichment of relatively fluid-mobile elements (Rb, K, Ba), and because enrichments increase in proportion to inferred mineral-melt incompatibility, it is likely that the patterns for ne-IPB/LKT and hy-IPB/LKT ratios reflect [1] different degrees of source enrichment by silicate melts (as opposed to aqueous fluids) and/or [2] different degrees of source depletion by melt removal. Thus the IPB lavas may sample mantle sources of varied enrichment. As seen in text Figure 5, the inferred sources are similar to those of many intraplate basalts (i.e., enriched MORB to OIB in nature), and dissimilar to common arc calcalkalic basalts. This view is supported by lack of [1] enrichment of highly fluid-mobile elements like B in virtually all Cascades basalts (Leeman et al, 2004; Manea et al., 2014), and [2] $^{238}U/^{232}Th$ disequilibria in most Cascades lavas (e.g., Volpe and Hammond, 1991; Jicha et al., 2009; Mitchell and Asmerom, 2011). These observations suggest that contributions of slab-derived fluids to magma sources are exceptionally low in this volcanic arc, and that flux-melting is likely subordinate to decompression melting.

We also compare MSH basaltic lavas to prevalent primitive magma types in the region (cf. Supplement Table S3). When normalized to the closely similar primitive LKT average, MSH Group A lavas are enriched at least two-fold in Rb, K, and Ba. Based on our mixing interpretation, this and less dramatic enrichments in other incompatible elements could result from incorporation of 'andesitic' material in the magma conduit system. Normalization of the Group B1 and B2 MSH subtypes to their postulated parental magma types (ne-IPB; Supplement Figure S4) shows that they have relatively flat compositional profiles close to unity for most elements plotted. We surmise that Groups A and B parental magmas form from distinct mantle sources (cf. Supplement

Note 7). The most incompatible elements (Rb, K, Ta, Nb, Ba) are enriched more than 2-fold in IPB-like Group B1 and B2 lavas relative to LKT-like Group A lavas and LREE, P, Sr, Zr, Hf, and Ti are also enriched to lesser degree, whereas Ni and Cr contents are comparable. These patterns (also see text Figs. 3 and 5) preclude a genetic connection between MSH IPBs and LKTs.

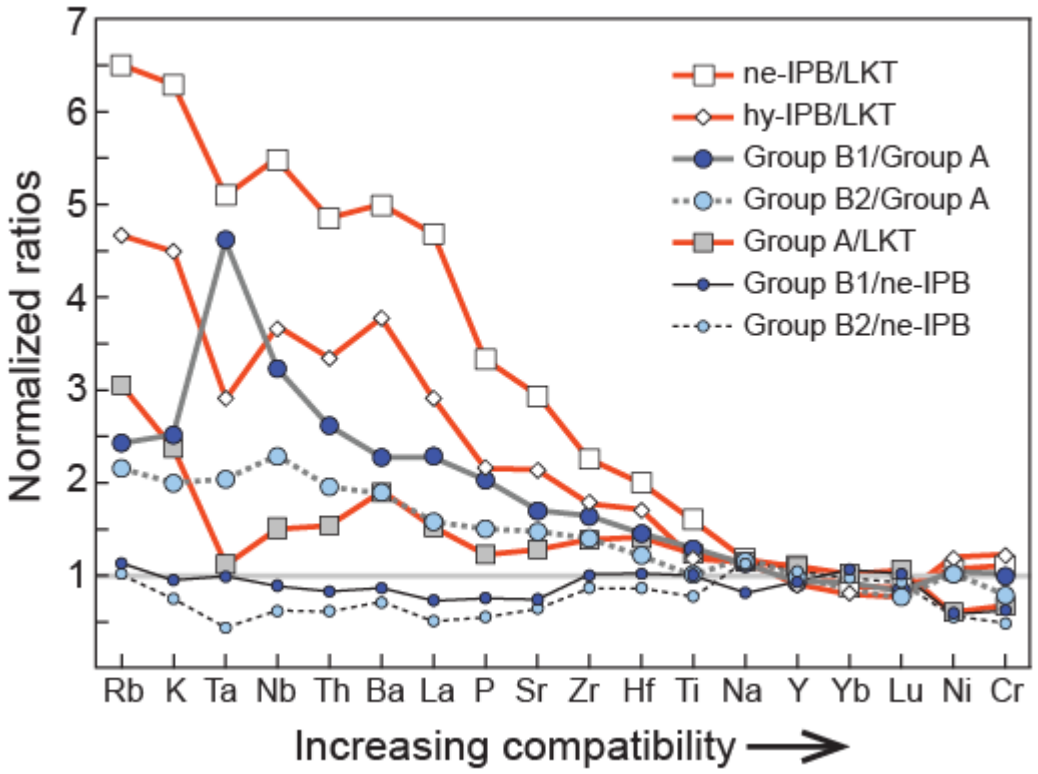

Supplement Figure S4. Trace element profiles showing relative differences between average compositions of basalts from MSH Groups A, B1 and B2 (omitting samples with SiO_2 > 53 wt%) and CCT primitive basalt types: ne-IPBs, hy-IPBs, and LKTs. All profiles represent ratios between the respective magma types as shown in the legend.

REFERENCES

Jicha, B.R., Hart, G.L., Johnson, C.M., Hildreth, W., Beard, B.L., Shirey, S.B., and Valley, J.W. (2009) Isotopic and trace element constraints on the petrogenesis of lavas from the Mount Adams volcanic field, Washington. Contributions to Mineralogy and Petrology, 157, 189-207.

Leeman, W.P., Tonarini, S., Chan, L.H., and Borg, L.E. (2004) Boron and lithium isotopic variations in a hot subduction zone – the southern Washington Cascades. Chemical Geology, 212, 101-124.

Manea, V.C., Leeman, W.P., Gerya, T., Manea, M., and Zhu, G. (2014) Subduction of fracture zones controls mantle melting and geochemical signature above slabs, Nature Communications, 5, 5095, doi:10.1038/ncomms6095

Mitchell, E.C., and Asmerom, Y. (2011) U-series isotope systematics of mafic magmas from central Oregon: Implications for fluid involvement and melting processes in the Cascade arc. Earth and Planetary Science Letters, 312, 378-389, doi:10.1016/j.epsl.2011.09.060.

Volpe, A.M., and Hammond, P. (1991) ^{238}U-^{230}Th-^{226}Ra disequilibria in young Mount St. Helens rocks: Time constraint for magma formation and crystallization. Earth and Planetary Science Letters, 107, 475-486.

Supplement Note 7. Primitive magma segregation conditions

Supplement Table S7 presents the results of olivine-addition back calculations to approximate compositions of parental magmas to representative regional primitive magma types (full data included in text Table 1 and Supplement Table S1). For each sample, analyses were first normalized to 100% total with Fe_2O_3 and FeO allocated according to X-fe3 = 0.15. Then, equilibrium olivine was added incrementally in small steps until Mg#s of the calculated liquid compositions reached values in equilibrium with olivine X_{Fo} values of 0.90, 0.91 and, for most, 0.92 (i.e., source Mg#s of 90, 91, and 92). Results at these steps are shown in Table S7. Parameters of note include (1) weight fraction of solid (olivine) added, (2) predicted olivine composition (X_{Fo}), (3) temperatures and pressures calculated at each stage using a variety of models as labeled (see below); these represent potential conditions under which the primitive liquids hypothetically could have last equilibrated with a peridotitic (i.e., ol + opx ± cpx ± others) mantle source. The redox state was held constant (X-fe3 = 0.15; near QFM redox buffer), and olivine-liquid Fe-Mg K_D value varied with liquid composition according to the model of Tamura et al. (2002).

Temperatures and pressures were estimated using a variety of geothermobarometers as noted in Supplement Table S7 (Albaréde, 1992 [as corrected by Leeman et al., 2005]; Sugawara, 2000; Putirka, 2008; Lee et al., 2009; Plank and Forsyth, 2016). The primary assumption in these calculations is that the primitive liquid (back-calculated as above) is in equilibrium with olivine and opx ± cpx. Similar P-T estimates are obtained by all the methods tested, and the Lee et al. estimates are considered representative. For example, for the primitive LKT, hy- or ne-normative IPBs, and SHO lavas corrected to Mg#90, all of the above methods shown yield average temperature estimates (SD ≤ 22°) within 15°C of the Lee et al. value. Average pressure estimates (S.D. ≤ 0.2 GPa) also agree with the Lee et al. value within 0.05 GPa.

Diagram on right side of the spreadsheet (cell L53, Supplement Table S7) depicts equivalent depth and temperature conditions at which the LKT, hy-IPB, and ne-IPB primitive melts could have hypothetically last equilibrated with mantle sources with Mg#s of 90, 91, and 92. All are above the dry mantle solidus of Hirschmann (2000),

which implies that they are products of near-anhydrous sources. If MSH parental magmas were derived by melting sources of similar Mg# (e.g., 90), then the LKTs appear to have segregated from greater depth (ca. 80 km) than the two IPB variants (ca. 50-60 km). Source Mg# for the IPBs would have to be near 91.5, and LKT source near 90 for their sources to be at similar depths (in which case their gross geochemical differences would be difficult to explain). Calculations for the shoshonite (SHO) are not plotted, but are included to illustrate the high Mg/Fe nature of this magma type (also shared with other regional calcalkalic magma varieties). Calculated (and sometimes observed) olivines in these magmas approach or exceed Fo_{89-90}, which suggests that their mantle sources have distinctly higher Mg# than those of the LKT and IPB magma types (cf. Leeman et al., 2005). Even for source Mg#92, apparent segregation depth for SHO sample DS-42-81 is less than 50 km, in which case it could be derived from shallow refractory mantle, or from a significantly different source lithology. But this is a topic for another paper.

Finally, using the PRIMELT3 spreadsheet of Herzberg and Asimow (2015), only the primitive LKT average composition appears to be compatible with having a spinel lherzolite mantle source. In contrast, the primitive ne-IPB and hy-IPB (and all CA type) basaltic compositions appear to require more pyroxene-rich sources. These observations support the view that the respective magma types derive from sources of distinct lithology. A key discriminant is the CaO content of these magmas. Notably, CaO is buffered by the presence of clinopyroxene. Thus, systematically higher CaO in Group A lavas seems consistent with relatively low clinopyroxene content in the source(s) of these magmas.

REFERENCES

Albaréde, F. (1992) How deep do common basaltic magmas form and differentiate? Journal of Geophysical Research, 97, 10997–11009.

Herzberg, C., and Asimow, P.D. (2015) PRIMELT3 MEGA.XLSM software for primary magma calculation: Peridotite primary magma MgO contents from the liquidus to the solidus, Geochemistry, Geophysics, and Geosystems, 16, 563–578, doi:10.1002/2014GC005631.

Hirschmann, M.M. (2000) Mantle solidus: Experimental constraints and the effects of peridotite composition. Geochemistry, Geophysics, and Geosystems, 1, 1042, doi:10.1029/2000GC000070.

Lee, C.-T.A., Luffi, P., Plank, T., Dalton, H., and Leeman, W.P. (2009) Constraints on the depths and temperatures of basaltic magma generation on Earth and other terrestrial planets using new thermobarometers for mafic magmas. Earth and Planetary Science Letters, 279, 20-33.

Leeman, W.P., Lewis, J.F., Evarts, R.C., Conrey, R.M., and Streck, M.J. (2005) Petrologic constraints on the thermal structure of the Cascades arc. Journal of Volcanology and Geothermal Research, 140, 67-105.

Plank, T., and Forsyth, D.W. (2016) Thermal structure and melting conditions in the mantle beneath the Basin and Range province from seismology and petrology. Geochemistry, Geophysics, Geosystems, 17, doi:10.1002/2015GC006205.

Putirka, K.D. (2008) Thermometers and barometers for volcanic systems. Reviews in Mineralogy and Geochemistry, 69, 61-120.

Sugawara, T. (2000) Empirical relationships between temperature, pressure, and MgO content in olivine and pyroxene saturated liquid. Journal of Geophysical Research, 105, 8457-8472.

Tamura, Y., Tatsumi, Y., Zhao, D., Kido, Y., and Shukuno, H. (2002) Hot fingers in the mantle wedge; new insights into magma genesis in subduction zones. Earth and Planetary Science Letters, 197, 105-116.